

Self-enrichment of Galactic halo globular clusters: stimulated star formation and consequences for the halo metallicity distribution

Geneviève Parmentier ^{*}*Institute of Astrophysics and Geophysics, University of Liège, 4000 Liège, Belgium*

Accepted Received ... ; in original form ...

ABSTRACT

We explore the self-enrichment hypothesis for globular cluster formation with respect to the star formation aspect. Following this scenario, the massive stars of a first stellar generation chemically enrich the globular progenitor cloud up to Galactic halo metallicities and sweep it into an expanding spherical shell of gas. This paper investigates the ability of this swept proto-globular cloud to become gravitationally unstable and, therefore, to seed the formation of second generation stars which may later on form a globular cluster. We use a simple model based on a linear perturbation theory for transverse motions in a shell of gas to demonstrate that the pressures by which the progenitor clouds are bound and the supernova numbers required to achieve Galactic halo metallicities support the successful development of the shell transverse collapse. Interestingly, the two parameters controlling the metallicity achieved through self-enrichment, namely the number of supernovae and the external pressure, also rule the surface density of the shell and thus its ability to undergo a transverse collapse. Such a supernova-induced origin for the globular cluster stars opens therefore the way to the understanding of the halo metallicity distributions. This model is also able to explain the lower limit of the halo globular cluster metallicity.

Key words: globular clusters: general – Galaxy: halo – supernova remnants – stars: formation.

1 INTRODUCTION

Globular clusters (GC) are dense, massive and round-shaped groups of stars present in the vast majority of galaxies. In our Galaxy, the halo GCs were among the very first bound structures to form and their study provides therefore valuable information about the early Galactic evolution. Their formation is an exciting but yet unsolved problem. For instance, it is still an open question whether Galactic halo GCs formed out of gas already chemically enriched (*pre-enrichment* models, e.g. Harris & Pudritz 1994) or whether they produced their own heavy elements through an earlier generation of stars within the GC progenitor itself (*self-enrichment* models). In the second class of models, the issue of their formation is directly related to the origin of their metal content (Cayrel 1986; Brown, Burkert & Truran 1995; Parmentier et al. 1999). Such a feature makes the self-enrichment scenario especially appealing if we hypothesize that the GC progenitor clouds are made of primordial (i.e.

metal-free) gas, a reasonable assumption for the Old Halo GCs, i.e. the population of old and coeval (Rosenberg et al. 1999) halo GCs.

Regarding the origin of the proto-globular cluster clouds (PGCC), Fall & Rees (1985) suggested that they formed out of the collapsing protoGalaxy, as cold and dense clouds in pressure equilibrium with a hot and diffuse background. In the frame of this theory, the GC progenitor clouds are thermally supported (i.e. no additional support against gravitation due to magnetic fields and turbulence) and made of primordial gas. In order to explain the metallicities of halo GCs, Parmentier et al. (1999, hereafter Paper I) expanded the Fall & Rees (1985) model for GC formation by the self-enrichment picture. According to this one, a first stellar generation forms in the central regions of each PGCC. When the massive stars explode as Type II supernovae (SNeII), they chemically enrich the surrounding gas and sweep the cloud, turning it in an expanding shell of gas in which the formation of a second, chemically enriched, stellar generation may be triggered. These second generation stars form

* E-mail: parm@astro.unibas.ch

the proto-globular cluster.

The sweeping and compression of the interstellar medium by massive star explosions is not the sole mechanism invoked to account for star formation during the earliest stages of the Galactic evolution. Some other models assume a different origin for the trigger. For instance, following Vietri & Pesce (1995), the high pressure confining the GC gaseous progenitor leads to the propagation of a strong shock inwards the cloud, stimulating thereby the formation of new stars. On another side, Murray & Lin (1992) and Dungey (1997) suggested that the propagation of shock waves is promoted by cloud-cloud collisions. In a similar way, star forming clouds may have coalesced into larger units until they reach a density and/or accumulated mass high enough to enable the formation of bound globular clusters (Larson 1988, Smith 1999). Obviously, several processes are able to collect ambient gas into dense layers/clouds where star formation can thereafter take place. Several of them may have been at work at the same time. Our interest being in understanding the origin of the metal content of GCs, in what follows, we investigate the hypothesis of star formation in gas layers swept by the explosions of PopIII massive stars located at the center of the PGCCs.

The debate of how PopIII stars looked like has been raging for many years. Numerous studies have addressed the issue of the collapse and fragmentation of primordial gas clouds in order to estimate the masses of PopIII stars. The primordial gas being deficient in heavy elements (i.e., the most efficient coolants in present-day star forming clouds), all of them have emphasized the importance of cooling by H_2 molecules. In spite of this, the achieved conclusions do not necessarily converge. Recent numerical simulations (Abel, Bryan & Norman 2002) suggest that metal-free stars form in isolation and are massive ($30 \lesssim M \lesssim 100 M_\odot$) objects. From their own simulations, Bromm, Coppi & Larson (1999) quoted a characteristic mass even larger than $100 M_\odot$. These results are in marked contrast with the early study performed by Palla, Salpeter & Stahler (1983) following which primordial gas clouds should be capable of fragmenting into low-mass stars (i.e., down to $\sim 0.1 M_\odot$). Nakamura & Umemura (1999) reached a somewhat intermediate conclusion. According to them, the mass range of the first stars is similar to its present value (i.e. no star with $M \gtrsim 100 M_\odot$) but nevertheless excludes low-mass long-lived stars, that is, the lowest mass star allowed to form in a metal-free medium is a $\simeq 3 M_\odot$ star. In a more recent model, Nakamura & Umemura (2001) predict a bimodal initial mass function for PopIII stars. In fact, the initial mass function of metal-free stars would show two distinct peaks at $\simeq 1 M_\odot$ and $\simeq 100 M_\odot$, that is, it would include intermediate mass ($1 \lesssim M \lesssim 10 M_\odot$) stars, massive ($10 \lesssim M \lesssim 100 M_\odot$) stars as well as very massive ($M \gtrsim 100 M_\odot$) ones. As quoted by Christlieb et al. (2003), the recent discovery of HE 0107-5240, the most metal-poor ($[Fe/H] = -5.3$) star ever discovered in the Galactic halo, could be a challenge to these models precluding the formation of stars with mass low enough for their life duration to exceed a Hubble time.

While there is currently a wide consensus that present star formation operates predominantly in a clustered mode (Lada, Strom & Myers 1993), the question whether clus-

ters of metal-free stars managed to form in the first (proto-) galaxies is still open. In this paper, we assume that at least some of the primordial star formation sites produced stellar *clusters* whose most massive stars ($10 \lesssim M \lesssim 50 M_\odot$) end their life as canonical SNeII. Therefore, our study does not include the possibility of a prompt enrichment of the primordial interstellar medium by a population of very massive (i.e., $\gtrsim 100 M_\odot$) stars as suggested by, e.g., Wasserburg & Qian (2000). The chemical enrichment provided by isolated (very) massive objects will be qualitatively discussed in Sect. 3 where we will see that they may be appropriate to account for the formation of very metal-poor stars, i.e., stars more metal-poor than the most metal-deficient halo GCs ($[Fe/H] \lesssim -2.5$).

Supernovae having long been thought to disrupt the cloud of gas out of which they have formed, Parmentier et al. (1999) studied the ability of pressure-truncated clouds to retain SNII ejecta. This ability will rule the metal content of the proto-cluster. In fact, in this class of models, the final metallicity is determined by the number of supernovae (N , which, assuming a given initial mass function and given SNII yields, determines the amount of metals dispersed within the PGCC) and the background pressure (P_h , which determines the mass of the cloud, that is, the mass of primordial gas to be chemically enriched). Comparing the gravitational energy of the PGCC with the kinetic energy of the supershell resulting from the SNII explosions, Parmentier et al. (1999) showed that the gaseous GC progenitors can sustain up to ~ 200 supernovae (the disruption criterion, Eq. 14, Paper I). This is a number high enough for the PGCCs to achieve halo metallicities. Furthermore, for a given number of exploding massive stars, a self-enrichment episode in pressure-bound clouds lead to a metallicity gradient throughout the resulting system of GCs and to a correlation between the mass and the achieved metallicity of the gaseous progenitors in the sense that the least massive clouds are the most metal-rich. Such a trend emerges because if the bound pressure is higher, the mass of the pressure-truncated cloud will be lower, and its ability to retain supernova ejecta will be greater. These trends, i.e. a metallicity gradient and a mass-metallicity relation, are indeed statistically present in the Old Halo, that is, the halo from which the presumably accreted component has been removed (Parmentier et al. 2000, Parmentier & Gilmore 2001).

After having analysed to which extent the Galactic halo GC data fit the correlations induced by the self-enrichment process, the next step is to wonder whether there are some stars forming out of the chemically enriched supershell, i.e. whether there is a second stellar generation tracing these correlations. The idea of star formation induced by supernova explosions dates back at least to Opik (1953). Numerous cases of distant star forming loops, connected with shells resulting from supernova explosions and located in the Galactic disc as well as in dwarf galaxies, are detailed in the literature (e.g. Comeron & Torra 1994, Walter et al. 1998, Efremov & Elmegreen 1998, Rubio et al. 1998). In this paper, we address the specific case of supershells made of swept PGCCs and within which the formation of the stars of future GCs may be triggered. In a first step, we limit our study to the propagation of the shell throughout the hot protogalac-

tic background in which the PGCCs are initially embedded, this part of the shell propagation being much longer than the propagation throughout the cloud (see Fig. 1).

The outline of the paper is as follows. In Sect. 2, we solve the perturbed equations of continuity and motion for transverse flows within the shell (i.e. the swept cloud) in order to identify the conditions supporting a successful shell transverse collapse. We also discuss in turn the impact of the different parameters acting upon the shell collapse and, thus, upon the temporal growth of the shell fragments in which further star formation may be stimulated. In Sect. 3, we show how the conditions required to stimulate a star formation episode within the shell provides a natural explanation to the observed metallicity range of halo GCs and how the shape of their metallicity spectrum constitutes the next step to work on. Sect. 4 describes some effects which our forthcoming computations should take into account in order to refine the present model. Finally, our conclusions are presented in Sect. 5.

2 STIMULATED STAR FORMATION IN PROTO-GLOBULAR CLUSTER CLOUDS

The shell will in general contain perturbed (transverse) velocity components and perturbations in the column density whose development leads to the transverse collapse of the swept PGCC and, thereby, to the formation of a second stellar generation. We now derive the conditions to get such a collapsing shell. The elementary method described below is adopted.

2.1 Modelling the transverse collapse of the shell

The computations are based on the linear perturbed equations of continuity and motion for transverse flows in the shell (e.g. Elmegreen 1994).

The perturbed equation of continuity (mass conservation) is

$$\frac{\partial \sigma_1}{\partial t} = -2 \frac{V_s}{R_s} \sigma_1 - \sigma_0 \nabla_T v, \quad (1)$$

where subscript T means that the gradient component under consideration is the transverse one, and the perturbed equation of motion (momentum conservation) is

$$\sigma_0 \frac{\partial v}{\partial t} = -\sigma_0 \frac{V_s}{R_s} v - c_s^2 \nabla \sigma_1 + \sigma_0 g_1. \quad (2)$$

In these equations, R_s and V_s are respectively the radius and the velocity of the shell, σ_0 is the unperturbed surface density, σ_1 is the perturbed surface density, v is the perturbed (transverse) velocity, c_s is the velocity dispersion of the material inside the shell, g_1 is the perturbed gravity, this one being related to the surface density through (Elmegreen 1994):

$$g_1 = -2\pi i G \sigma_1. \quad (3)$$

As mentioned above, the evolution of the shell is studied while propagating through the hot background, i.e. when the whole cloud has been swept inside the shell. The hot background being a diffuse medium, the shell mass $M_s(t)$ does not increase any longer at this stage of its propagation

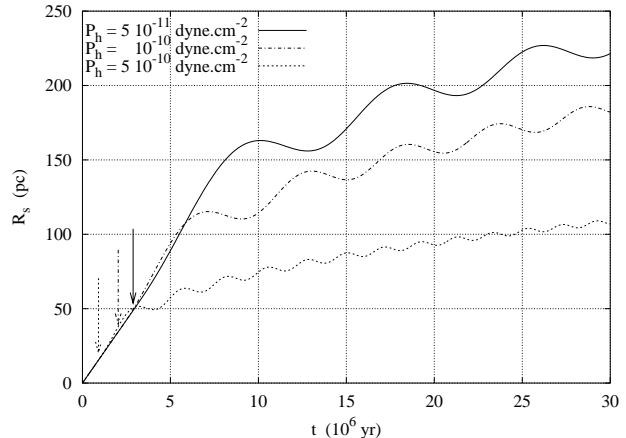


Figure 1. Evolution with time of the shell radius inferred from Eqs. (5 - 8) assuming that 200 SNeII explode at a constant rate during 30 million years and for three different hot protogalactic background pressures, from top to bottom 5×10^{-11} (plain curve), 10^{-10} (dashed-dotted curve) and 5×10^{-10} dyne.cm $^{-2}$ (dotted curve). In each case, an arrow indicates the time t_{em} at which the shell crosses the interface between the cold and hot phases

and is given by the mass M of the progenitor cloud. The unperturbed surface density of the shell is thus given by

$$\sigma_0 = \frac{1}{4\pi} \frac{M_s(t)}{R_s^2} = \frac{1}{4\pi} \frac{M}{R_s^2}. \quad (4)$$

Equation 1 shows that the development with time of any perturbation of the shell surface density ($\partial \sigma_1 / \partial t > 0$) is inhibited by the stretching of the perturbed region due to the shell expansion (i.e. $V_s > 0$, first term on the right hand-side, hereafter rhs) while the convergence of the perturbed flows supports the growth of the perturbation (second term on the rhs). Equation 2 shows that an initial transverse flow of material along the shell develops ($\partial v / \partial t > 0$) only if the self-gravity (third term on the rhs) overcomes the stabilizing effects of the stretching (first term on the rhs) and of the internal pressure (second term on the rhs), here represented by c_s^2 , the shell sound speed squared.

In order to solve Eqs.1 and 2 properly, we now turn to the determination of the expansion law of the shell, i.e. $R_s(t)$ and $V_s(t)$, while it propagates throughout the hot protogalactic background.

2.2 Supershell propagation throughout the hot background

The equations describing the propagation of a supernova-driven shell are as follow (Castor et al. 1975).

(i) The supernova explosions add energy to the bubble at a constant rate \dot{E}_o and the dominant energy loss of the bubble comes from the work against the dense shell, hence the variation with time of the energy E_b of the bubble obeys

$$\dot{E}_b = \dot{E}_o - 4\pi R_s^2 P_b \dot{R}_s. \quad (5)$$

We assume that the kinetic energy of every SN is 10^{51} ergs and that the SN phase lasts about thirty million years, i.e. $\dot{E}_o = N 10^{51}$ ergs/30Myr.

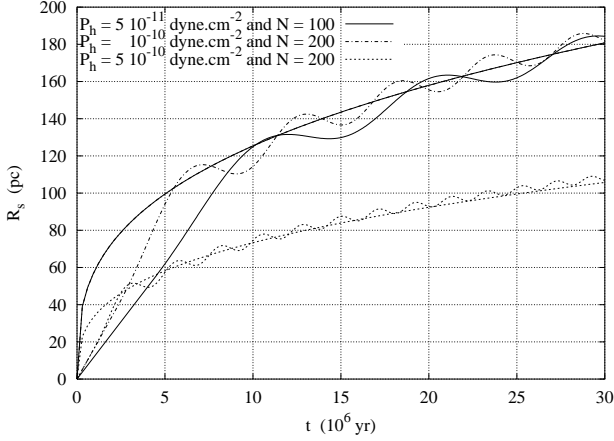


Figure 2. Comparison between the evolution with time of the shell radius computed from Eqs. (5 - 8) and the average radius given by Eq. 9 (i.e. $\langle R_s(t) \rangle \propto t^{1/3}$) for the quoted numbers N of SNeII and background pressures P_h

(ii) The internal energy E_b and the pressure P_b of the bubble are related through

$$\frac{4\pi}{3} R_s^3 P_b = \frac{2}{3} E_b, \quad (6)$$

(iii) The shell motion obeys Newton's second law

$$\frac{d}{dt} [M_s(t) \dot{R}_s(t)] = 4\pi R_s^2 (P_b - P_{ext}) - \frac{GM_s^2(t)}{2R_s^2(t)}, \quad (7)$$

where P_{ext} is the pressure of the medium just outside the shell.

(iv) Considering the case of swept PGCCs propagating through the hot protogalactic background, the mass of the shell is constant in time and is given by the mass of the cloud (see Sect. 2.1):

$$M_s(t) = M. \quad (8)$$

The pressure external to the shell is exerted by the surrounding hot background (i.e. $P_{ext} = P_h$ in Eq. 7) and is therefore assumed to be constant in time. This pressure will strongly decelerate the shell as illustrated below. Numerical resolution of Eqs. (5 - 8) provides $R_s(t)$ and thereby $V_s(t)$ and $\sigma_0(t)$. The initial conditions are those at the time t_{em} , i.e. when the shell crosses the interface between the cloud and the surrounding background: the mass and radius of the shell are those of the pressure-bound cloud ($R_s(t_{em}) = R$, $M_s(t_{em}) = M$), the velocity of the shell is determined by its former propagation at constant speed V through the cloud (see Paper I, Eq. 13), that is $V_s = V$ and $A_s = 0$.

Figure 1 shows the evolution with time of the shell radius for 200 SNeII, i.e. the maximum number of supernovae that a PGCC can sustain (disruption criterion, Paper I), and for 3 different values of the hot protogalactic background pressure, i.e. $P_h = 5 \times 10^{-11}$, 10^{-10} and 5×10^{-10} dyne.cm $^{-2}$. The SN rate being the same in the three cases, the shells propagate at the same velocity in the cold phase (Eq. 13 in Paper I). Their expansions begin to differ once they have crossed the interface between their respective PGCC and the hot background in which the latter is embedded, this

time being indicated by an arrow in Fig. 1. Obviously, the propagation of the shell through the cloud is much shorter than its propagation through the background. A significant part of the shell expansion through the background takes place at early time. Indeed, after a transient phase during which the velocity of the shell does not differ markedly from its velocity inside the cloud (Fig. 1), the overall expansion slows down and the radius of the shell scales roughly as $t^{1/3}$. This average expansion can be obtained from Eqs. (5 - 8) assuming that $M_s(t) = 0$, reflecting thereby that the temporal evolution of the shell radius does not depend strongly on the mass (Brown et al. 1995):

$$\langle R_s(t) \rangle = \left(\frac{3}{10\pi} \frac{\dot{E}_o}{P_h} \right)^{1/3} t^{1/3}. \quad (9)$$

Figure 2 shows the good agreement between Eq. 9 and the result of the numerical integration over time of Eqs. (5 - 8). Equation 9 shows that, during the long-term evolution, the expansion rates of two shells having the same (N/P_h) ratio are similar. Figure 2 illustrates this effect for two sets of values, namely $N=100$ and $P_h=5 \times 10^{-11}$ dyne.cm $^{-2}$ (plain curve) and $N=200$ and $P_h=10^{-10}$ dyne.cm $^{-2}$ (dashed-dotted curve).

2.3 Growth with time of the shell fragments

In order to assess whether the shell transverse collapse proceeds successfully or not, we now numerically integrate over time Eqs.1 and 2 in order to derive the temporal evolutions of the perturbed and unperturbed surface densities, $\tilde{\sigma}_1(t)$ and $\sigma_0(t)$, respectively.

Assuming that the perturbed quantities follow a complex exponential of the angular position ϕ along the shell, we get:

$$\sigma_1(t, \phi) = \tilde{\sigma}_1(t) e^{-i\eta\phi} \quad (10)$$

and

$$v(t, \phi) = \tilde{v}(t) e^{-i\eta\phi} e^{i\Delta\phi}. \quad (11)$$

In these equations, $\Delta\phi$ represents the phase difference between the perturbed surface density σ_1 and the perturbed velocity v . η is the angular wavenumber and is related to the spatial wavenumber k by:

$$\eta = kR_s = \frac{2\pi}{\lambda} R_s \quad (12)$$

where λ is the wavelength of the perturbation, namely the average distance between forming fragments, the sites of future star formation. Therefore, η is the number of forming clumps along a shell circumference and, as such, η must be an integer. Moreover, any realistic perturbation must fit inside a fraction of the shell circumference, say, $\lambda \leq R_s$ or $\eta \geq 6$.

At a time t and an angular position ϕ along the shell, the shell surface density σ_s obeys

$$\sigma_s(t, \phi) = \sigma_0(t) + \sigma_1(t, \phi) = \sigma_0(t) + \tilde{\sigma}_1(t) \cos(\eta\phi). \quad (13)$$

The fragmentation of the shell, i.e. its fully developed transverse collapse, occurs when

$$\tilde{\sigma}_1(t) = \sigma_0(t). \quad (14)$$

Writing $-i\eta/R_s$ for the gradient and using Eqs. 3 and 4, Eqs. 1 and 2 successively become:

▷ Perturbed equation of continuity:

$$\begin{aligned} \frac{\partial \tilde{\sigma}_1}{\partial t} &= -2 \frac{V_s}{R_s} \tilde{\sigma}_1 + \sigma_0 \frac{i \eta}{R_s} \tilde{v} e^{i\Delta\phi} \\ \frac{\partial \tilde{\sigma}_1}{\partial t} &= -2 \frac{V_s}{R_s} \tilde{\sigma}_1 + \frac{i \eta M}{4\pi R_s^3} \tilde{v} e^{i\Delta\phi} \end{aligned} \quad (15)$$

▷ Perturbed equation of motion:

$$\begin{aligned} \sigma_0 e^{i\Delta\phi} \frac{\partial \tilde{v}}{\partial t} &= -\sigma_0 \frac{V_s}{R_s} \tilde{v} e^{i\Delta\phi} + c_s^2 \frac{i \eta}{R_s} \tilde{\sigma}_1 \\ &\quad - 2\pi i G \sigma_0 \tilde{\sigma}_1 \\ \frac{\partial \tilde{v}}{\partial t} &= -\frac{V_s}{R_s} \tilde{v} + \frac{4 \pi i \eta c_s^2}{M} R_s \tilde{\sigma}_1 e^{-i\Delta\phi} \\ &\quad - 2\pi i G \tilde{\sigma}_1 e^{-i\Delta\phi} \end{aligned} \quad (16)$$

Seven parameters intervene in the ability of the shell to undergo a transverse collapse:

- the supernova number N and the pressure external to the shell P_h , which determine the shell expansion law (R_s depends on N and P_h) and mass (M depends on P_h),
- the initial values of the perturbed quantities, $\tilde{\sigma}_1(t_{em})$ and $\tilde{v}(t_{em})$, and the associated phase difference $\Delta\phi$,
- the number η of forming clumps embedded along a shell circumference,
- the velocity dispersion c_s of the shell material which is related to the internal pressure P_s of the shell, supporting it against transverse collapse, through $P_s = c_s^2 \rho_s$ (ρ_s is the volumic mass density of the shell material).

In what follows, the influence of each of the parameters involved in the fragmentation process is investigated, the final aim being to check whether some reasonable sets of conditions can lead to the shell fragmentation.

2.3.1 The phase difference between v and σ_1 : $\Delta\phi$

The amplitude of the perturbed surface density at a time t , $\tilde{\sigma}_1(t)$, results from its initial value $\tilde{\sigma}_1(t_{em})$ and from the transverse flows which redistribute the shell mass accumulated while the shell was propagating throughout the progenitor cloud. The fragmentation is therefore favoured if these transverse flows converge towards the clumps initially present within the shell. Such a situation corresponds to a phase difference $\Delta\phi = -\pi/2$ between the two perturbed quantities $\sigma_1(t, \phi)$ and $v(t, \phi)$, that is, the transverse velocity exhibits a phase delay of a quarter of a wavelength with respect to the perturbed surface density (see Fig. 3). Replacing $\Delta\phi$ by this value, Eqs. 15 and 16 respectively become:

$$\frac{\partial \tilde{\sigma}_1}{\partial t} = -2 \frac{V_s}{R_s} \tilde{\sigma}_1 + \frac{\eta M}{4\pi R_s^3} \tilde{v}, \quad (17)$$

$$\frac{\partial \tilde{v}}{\partial t} = -\frac{V_s}{R_s} \tilde{v} - \frac{4 \pi \eta c_s^2}{M} R_s \tilde{\sigma}_1 + 2\pi G \tilde{\sigma}_1. \quad (18)$$

In what follows, the roles of the other parameters is studied assuming that $\Delta\phi = -\pi/2$, i.e. through the numerical integration of Eqs. 17 - 18.

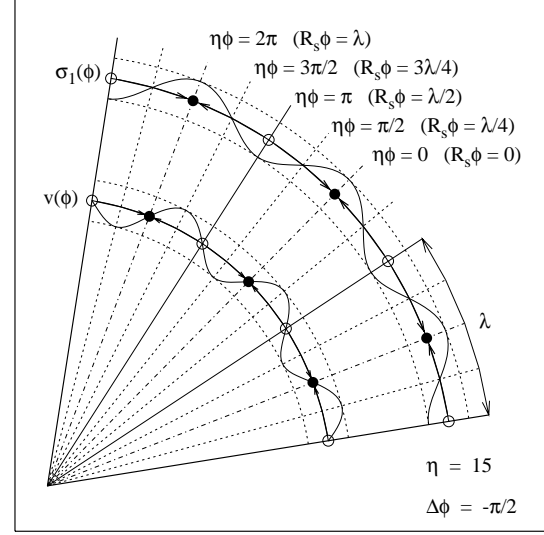


Figure 3. Schematic description of the sinusoidal (i.e. complex exponential) behaviour with ϕ of the perturbed quantities v (lower curve) and σ_1 (upper curve) along a fraction of the shell circumference at a given time assuming that the number of clumps η is 15 and the phase difference $\Delta\phi$ between v and σ_1 is $-\pi/2$. Such a phase difference corresponds to the convergence of the transverse (perturbed) flows (indicated by the thick arrows) towards the initial clumps (filled circles). The open circles represent the shell regions which are progressively depleted by the transverse flows

2.3.2 The global parameters: N and P_h

In order to assess whether the shell fragments or not during its propagation through the hot protogalactic background, we compare in Fig. 4 the evolutions with time of the perturbed and unperturbed surface densities, namely $\tilde{\sigma}_1(t)$ and $\sigma_0(t)$, for different values of the external pressure P_h (5×10^{-10} and 10^{-10} dyne.cm $^{-2}$) and numbers N of SNeII (100 and 200). The corresponding metallicity is indicated in each panel. The other parameters are kept the same in every case: the sound speed c_s of the shell material is 1 km.s^{-1} , the perturbed velocity $v(t_{em})$ is $0.01 V_s(t_{em})$, the number of forming clumps η is 10 and the initial perturbed surface density is assumed to be of order one per cent of the unperturbed value, namely $\sigma_1(t_{em}) = 0.01 \times \sigma_0(t_{em})$. This choice may seem rather arbitrary but the next paragraph will show that the initial amplitude of σ_1 does not affect the results significantly .

While the unperturbed surface density decreases due to the shell expansion at constant mass, the perturbed surface density grows at a rate which depends on the external pressure and on the number of SNeII. The comparison of the different panels in Fig. 4 shows that the development of $\tilde{\sigma}_1(t)$ with respect to $\sigma_0(t)$ is favoured by a *high background pressure* and a *low number of SNeII*. Among the three panels presented ($P_h = 10^{-10}$ dyne.cm $^{-2}$ and $N=100$, $P_h = 5 \times 10^{-10}$ dyne.cm $^{-2}$ and $N=100$, $P_h = 5 \times 10^{-10}$ dyne.cm $^{-2}$ and $N=200$), the transverse collapse

of the shell is successfully achieved¹ when the lower number of supernovae is combined with the larger external pressure ($P_h = 5 \times 10^{-10}$ dyne.cm⁻² and $N=100$). This effect comes from the dependence of the shell surface density on the external pressure P_h and the supernova number N . Indeed, combining the mass of a pressure-truncated gas cloud (i.e. $M \propto P_h^{-1/2}$) with Eq. 9, the surface density of the shell scales as:

$$\sigma_0(t) \propto \frac{M}{R_s(t)^2} \propto \frac{P_h^{1/6}}{N^{2/3}}. \quad (19)$$

Consequently, the larger the pressure and/or the lower the supernova number, the larger the shell surface density and the larger the growth rate of the perturbation (see Eq. 1 and Eq. 2, a larger surface density favours the terms promoting an efficient transverse collapse). *Therefore, although the presence of exploding massive stars is required to stimulate the formation of a second stellar generation, too large a number of SNeII inhibits the ability of the shell to collapse and to form new stars*².

The influence of the surface density of the shell on its collapse is reminiscent of the star formation law on large scales, i.e. averaged over entire galactic discs. In that case, providing that the gas surface density is larger than a density threshold, the star formation rate follows a power-law of the gas surface density (the so-called Schmidt law) while it falls sharply below (Kennicutt 1989). The threshold surface density varies from one galaxy to another but remains nevertheless in the range 10^{20} – 10^{21} cm⁻². It may not be a coincidence that the shell surface densities obtained in the frame of this model are of the same order of magnitude or even larger (see Sect. 2.3.3).

The dependence of the perturbation growth rate on N and P_h raises a point of interest, worthy of a mention here. It just so happens that the parameters determining the final metallicity of the proto-cluster, namely the number of supernovae (N , which determines the amount of metals dispersed within the PGCC) and the background pressure (P_h , which determines the mass of the cloud, that is, the mass of primordial gas to be chemically enriched) are also some of those influencing the ability of the shell to form new stars. *If some combinations of external pressures and SN numbers support the completion of the shell transverse collapse much more than some others do, then the formation of second stellar generations with the corresponding metallicities will be favoured.* Therefore, in the frame of the self-enrichment scenario, there is a direct link between the achieved metallicity and the probability of forming halo stars, i.e. *the study of*

the fragmentation process may shed light on the metallicity distribution function of Galactic halo field stars and GCs.

Figure 4 and Eq. 19 show that the shell fragmentation is favoured by a low number of SNe and a high pressure of the hot protogalactic background. Now, let us imagine that, on the contrary, the collapse efficiency increases with both decreasing number of SNeII and pressure. As P_h and N get smaller, the number of successful transverse collapses increases and the newly formed stars are more metal-poor. Thus, the metallicity distribution function of the Galactic halo would exhibit an increasing number of proto-clusters/halo stars with decreasing metallicity. If, on the other hand, the shell ability to achieve fragmentation increased with both increasing external pressure and SN number, then the larger P_h and N , the more numerous the transverse collapses and the more metal-rich the newly formed stars. As a result, there would be an increasing number of proto-clusters/halo stars with increasing metallicity. Neither an increasing nor a decreasing metallicity distribution function is observed for the Galactic halo. In contrast, the metallicity distributions, for both halo field stars (Laird et al. 1988) and halo GCs (Zinn 1985), are peaked-shape. While the finding that the shell transverse collapse is favoured by large external pressures (promoting “large”, i.e. mildly metal-poor, metallicities) and low SN numbers (supporting low metallicities) is not sufficient in itself to draw some definitive conclusions regarding the shape of the halo metallicity distribution, it appears that it does not contradict it either.

2.3.3 The initial perturbed surface density: $\tilde{\sigma}_1(t_{em})$

Protogalactic shells such as those studied here exhibit number surface densities of order several 10^{20} cm⁻². Indeed, using Eqs. 4 and 9, one gets:

$$\begin{aligned} \sigma_0(t, N, P_h) &\simeq 5 \times 10^{-3} P_{h(10)}^{1/6} N_{200}^{-2/3} t_6^{-2/3} \text{ g.cm}^{-2} \\ &\simeq 2.5 \times 10^{21} P_{h(10)}^{1/6} N_{200}^{-2/3} t_6^{-2/3} \text{ cm}^{-2} \end{aligned} \quad (20)$$

where the subscript (10) means that the pressure is expressed in units of 10^{-10} dyne.cm⁻², the subscript 200 means that N is expressed in units of 200 SNe and the subscript 6 means that the time is expressed in units of 10^6 years. Considering the interstellar medium of the Galactic disc with roughly the same surface density (though a bit lower, i.e. $\simeq 10^{20}$ cm⁻²), the relative non-uniformities in the number surface density are typically of order 0.01 - 0.2 (Wunsch & Palous 2001). However, the initial perturbation in the shell surface density is certainly not as large as some of the clumps of this *quiescent* disc interstellar medium since *turbulent mixing* is expected to take place within the shell (this is an important requirement to achieve the efficient mixing of the supernova heavy elements with the cloud gas and, therefore, to maintain the chemical homogeneity of the shell, that is, of the proto-globular cluster; see Brown et al. 1991), thus lowering the surface density inhomogeneities.

Figure 4 also shows the temporal evolution of σ_0 and $\tilde{\sigma}_1$ assuming that the initial perturbed surface density is lower than in Sect. 2.3.2, namely 0.25% $\sigma_0(t_{em})$ instead of 1% $\sigma_0(t_{em})$. Despite these different initial values, each panel displays almost identical $\tilde{\sigma}_1(t)$ curves in both cases. Owing

¹ At this point, it should be kept in mind that once the shell has achieved its complete transverse collapse, Eqs. 1 and Eqs. 2 are no longer valid. Therefore, once $\sigma_0 \leq \tilde{\sigma}_1$, the curve $\tilde{\sigma}_1(t)$ has no longer physical meaning.

² Unlike the protogalactic shells we study, the collapse of shells expanding in the Galactic disc is made easier by a larger number of SNeII. In fact, assuming that the surrounding interstellar medium is roughly homogeneous, i.e. the shell radius is smaller than the density scale-height of the Galactic HI layer, one gets by mass conservation, assuming a pre-shell density ρ_0 , $\sigma_0 = \frac{R_s \rho_0}{3}$. In this case, a larger number of SNeII leads to a larger radius at a given time and, therefore, to larger surface density and perturbation growth rate.

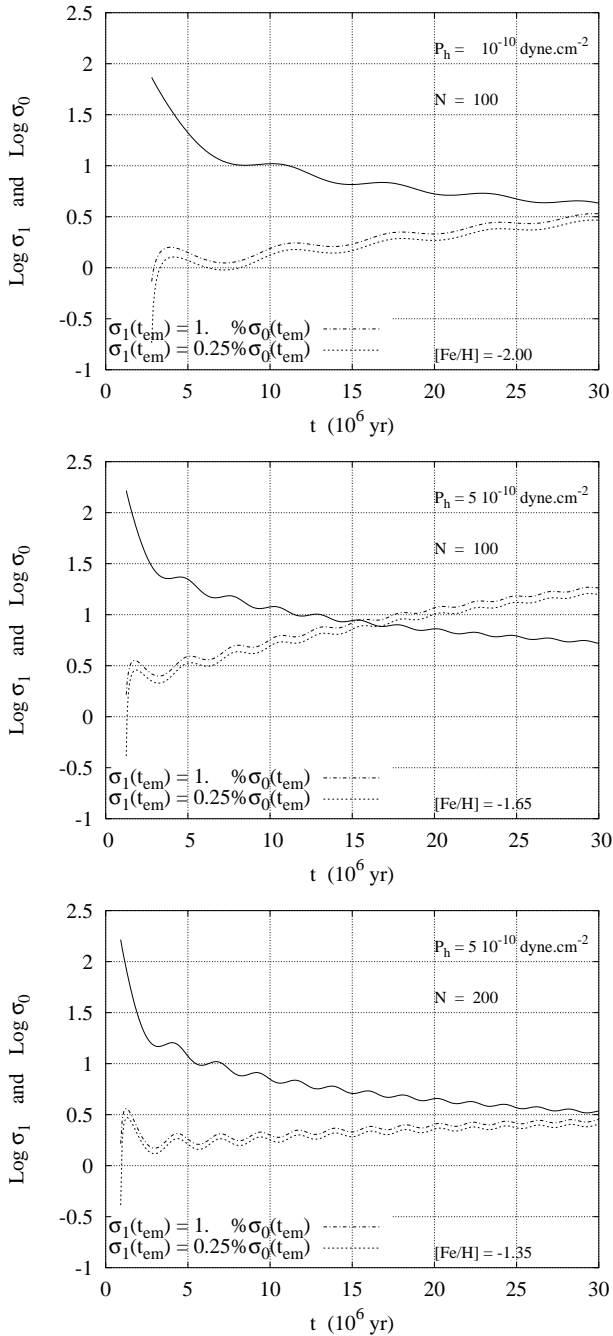


Figure 4. Temporal evolution of σ_0 (plain curves) and $\tilde{\sigma}_1$ (dashed-dotted curves), expressed in units of $1 M_{\odot} \cdot \text{pc}^{-2}$, considering two different initial perturbed surface densities (see the keys) and the external pressures and SNII numbers indicated. In each panel, $c_s = 1 \text{ km} \cdot \text{s}^{-1}$, $\eta = 10$ and $v(t_{em}) = 0.01 V_s(t_{em})$

to the initial transverse flows, the initial clumps quickly undergo a replenishment in shell material leading afterwards to very similar temporal evolutions of the perturbed surface density whatever the initial perturbed surface density. Obviously, this one is not a key parameter of the fragmentation process.

2.3.4 The initial perturbed velocity: $v(t_{em})$

All the results presented here above assume the spherical symmetry of the supershell. It is clear however that such a system is not expected to remain perfectly spherical. The deviations from spherical symmetry can arise, for instance, from the non point-like nature of the energy input, namely all the stars of the first generation cluster are not located exactly at the centre of the cloud/shell. A rough estimate of the initial amplitude of the transverse motions within the shell can therefore be derived from the size of this cluster. A star located at a distance r from the shell centre will induce a transverse velocity v such that:

$$v \simeq V_s \frac{r}{R_s}. \quad (21)$$

In order to estimate the size r of the cluster of massive stars hosted by a PGCC, we refer to R 136, the dense core of the 30 Doradus Nebula located in the Large Magellanic Cloud. The 30 Doradus nebula shows an impressive example of a two-stage stellar formation. The energetic activity of a very compact bright cluster, R136, which includes several tens of O stars, triggers the formation of a new stellar generation revealed by numerous infrared sources in or near some bright filaments west and northeast of R136 (Rubio et al. 1998). Based on Hubble Space Telescope photometry, Campbell et al. (1992) detected about 160 stars more massive than $10 M_{\odot}$ in R136 which they define as a region of $2.2 \text{ pc} \times 1.9 \text{ pc}$. This number of massive stars being remarkably similar to the numbers of SNeII used in our self-enrichment model, we adopt R136 as the most similar example in the Local Group of what may have been the first generation cluster. A radius of 1 pc appears therefore as a reasonable estimate of the size of this cluster, the source of the energy input.

Considering an average background pressure of $10^{-10} \text{ dyne} \cdot \text{cm}^{-2}$ and the corresponding cloud radius ($\simeq 30 \text{ pc}$, see Eq. 3, Paper I), the transverse velocity when the shell reaches the cloud boundary is:

$$v(t_{em}) \simeq \frac{1 \text{ pc}}{30 \text{ pc}} V_s(t_{em}) \simeq 0.03 V_s(t_{em}). \quad (22)$$

Figure 5 displays the evolution with time of σ_0 and $\tilde{\sigma}_1$ assuming three different values for the initial transverse velocity, namely $0.01 V_s(t_{em})$, $0.02 V_s(t_{em})$ and $0.03 V_s(t_{em})$, while keeping all the other parameters to their previous values. In sharp contrast with $\tilde{\sigma}_1(t_{em})$, $\tilde{v}(t_{em})$ appears to be an important parameter of the shell transverse collapse. For instance, considering the bottom panel in Fig. 5 ($P_h = 5 \times 10^{-10} \text{ dyne} \cdot \text{cm}^{-2}$ and $N=200$), the fragmentation takes place less than 15 million years after the first SN explosion if $v(t_{em}) = 0.03 V_s(t_{em})$, whereas it is prevented if $v(t_{em}) = 0.01 V_s(t_{em})$.

2.3.5 The number of forming clumps: η

In supernova-driven shells of gas, star formation does not take place all along the whole periphery but, instead, takes place in regularly spaced clumps (i.e., where the transverse collapse brings some gas from depleted adjoining regions in the shell, see Fig. 3). The number η of such clumps along a shell circumference is thus related to the wavelength λ

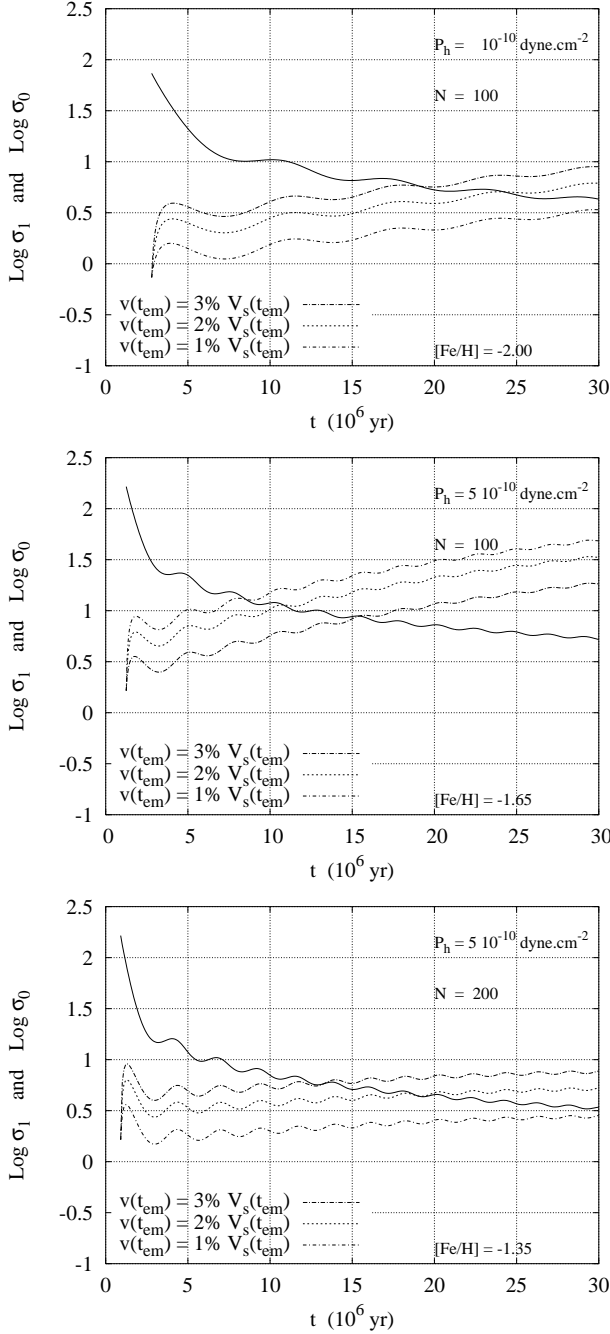


Figure 5. Temporal evolution of σ_0 (plain curves) and $\tilde{\sigma}_1$ (dashed-dotted curves), expressed in units of $1 M_{\odot} \cdot \text{pc}^{-2}$, considering three initial perturbed velocities (see the keys) and the external pressures and SNII numbers indicated. In each panel, $c_s = 1 \text{ km} \cdot \text{s}^{-1}$, $\eta = 10$ and $\tilde{\sigma}_1(t_{em}) = 0.01 \sigma_0(t_{em})$

of the perturbation (Eq. 12). This aspect of shell collapse modelling following which stars are formed in discrete stellar subsystems along a shell periphery is supported by several observations of star forming shells, the so-called Sextant being one of the most illustrative. In the Large Magellanic Cloud, a set of five OB associations are located along a HI supershell, sustaining there about 1/6 of a complete circle

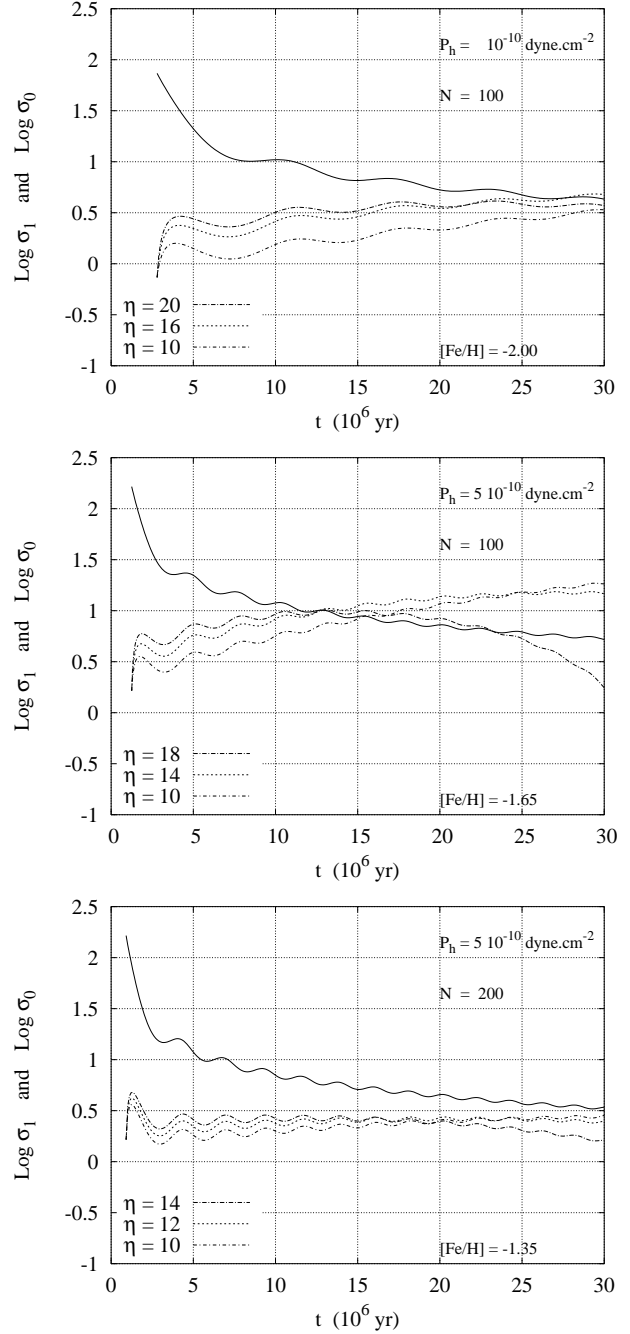


Figure 6. Temporal evolution of σ_0 (plain curves) and $\tilde{\sigma}_1$ (dashed and dotted curves), expressed in units of $1 M_{\odot} \cdot \text{pc}^{-2}$, considering the external pressures, SNII numbers and numbers of forming clumps indicated (see the keys). In each panel, $c_s = 1 \text{ km} \cdot \text{s}^{-1}$, $\tilde{\sigma}_1(t_{em}) = 0.01 \sigma_0(t_{em})$, $v(t_{em}) = 0.01 V_s(t_{em})$

and being thus called the Sextant (Efremov & Elmegreen 1998). Efremov, Ehlerova & Palous (1999) showed that the OB associations are regularly spaced, the deprojected average distance between two subsequent stellar groups being $\sim 37 \text{ pc}$. Furthermore, using numerical simulations of shells expanding in a mass model of the Large Magellanic Cloud, they concluded that the formation of these 5 OB associations is most probably the result of a triggered star forma-

tion episode in the supershell created by SNeII located near the Sextant centre. Their simulations also explain how projection effects make the visible star forming regions only a fraction of a total circle.

The influence of the number of clumps embedded within the shell on the transverse collapse is illustrated in Fig. 6. The parameter η is not as negligible as the initial perturbed surface density. In some cases, it acts upon the fragmentation process almost as strongly as the initial transverse velocity. It is thus worth estimating the angular wavenumbers which are the most favourable to the growth of an initial perturbation. In order to do so, we now derive an analytical approximation of the instantaneous growth rate of the perturbation. This is done straightforwardly by assuming that the perturbed quantities vary exponentially with time t , in analogy with the exponential growth rate found in other instability problems (e.g. the Jeans mass) even though there is no real exponential growth in this problem owing to the shell expansion and the corresponding time dependence of σ_0 . It is thus important to keep in mind that the perturbation growth rate derived below (Eqs. 28 and 31) is *not* used to compute the temporal evolution of σ_1 (the cases displayed in Fig. 6 are obtained from solving Eqs 17-18) but merely to derive η estimates favouring the shell collapse. The perturbed quantities are written:

$$\sigma_1(t, \phi) = \tilde{\sigma}_1(t_{em}) e^{\omega t} e^{-i\eta\phi} \quad (23)$$

and

$$v(t, \phi) = \tilde{v}(t_{em}) e^{\omega t} e^{-i\eta\phi} e^{i\Delta\phi}, \quad (24)$$

where ω is the angular frequency of the perturbation. Following Eqs. 23 and 24, we write ω for the time derivatives and $-i\eta/R_s$ for the transverse gradients. Therefore, Eqs. 1 and 2 become respectively

$$\omega\sigma_1 = -2\frac{V_s}{R_s}\sigma_1 + \sigma_0\frac{i\eta}{R_s}v \quad (25)$$

and

$$\sigma_0\omega v = -\sigma_0\frac{V_s}{R_s}v + c_s^2\frac{i\eta}{R_s}\sigma_1 - 2\pi iG\sigma_0\sigma_1, \quad (26)$$

using Eq. 3 in the latter.

The elimination of the perturbed quantities σ_1 and v between Eqs. 25 and 26 provides the dispersion equation, namely the relation between the angular frequency ω (i.e. the instantaneous growth rate) and the angular wavenumber η of the perturbation:

$$\sigma_0 \left(\omega + 2\frac{V_s}{R_s} \right) \left(\omega + \frac{V_s}{R_s} \right) - \sigma_0 \frac{i\eta}{R_s} \left(2\pi iG\sigma_0 - c_s^2 \frac{i\eta}{R_s} \right) = 0, \quad (27)$$

whose solution is given by

$$\omega(\eta) = -\frac{3}{2}\frac{V_s}{R_s} + \sqrt{\frac{3}{2}\frac{V_s^2}{R_s^2} + 2\pi G\sigma_0\frac{\eta}{R_s} - c_s^2\frac{\eta^2}{R_s^2}}. \quad (28)$$

Let us consider the *first growing mode*. This one corresponds to the sequence of values of η which maximises the angular frequency ω at each moment of the shell propagation, i.e. $\eta_{fg} = \eta(t)$ such that

$$\frac{d\omega}{d\eta} = 0. \quad (29)$$

Equation 29 indeed corresponds to a maximum since the discriminant of Eq. 28 shows a negative curvature with η . The instantaneous angular wavenumber and the instantaneous angular frequency associated to the first growing mode obey respectively

$$\eta_{fg} = \frac{\pi G}{c_s^2}\sigma_0 R_s = \frac{1}{4c_s^2}\frac{GM}{R_s} \quad (30)$$

and

$$\omega_{fg} = -\frac{3}{2}\frac{V_s}{R_s} + \sqrt{\frac{V_s^2}{R_s^2} + \frac{\pi^2 G^2 \sigma_0^2}{c_s^2}}. \quad (31)$$

Taking into account the dependence of M and R_s (Eq. 9) on P_h and N , Eq. 30 shows that η_{fg} depends on the external pressure P_h , on the SN number N and on time t as

$$\eta_{fg} \propto P_h^{-1/6} N^{-1/3} t^{-1/3}. \quad (32)$$

A first guess of a favourable angular wavenumber can be estimated from the temporal average of Eq. 30 over the time spent by the supershell in the hot protogalactic background:

$$\langle \eta_{fg} \rangle = \frac{1}{\Delta t - t_{em}} \int_{t_{em}}^{\Delta t} \eta_{fg}(t') dt', \quad (33)$$

where Δt is the duration of the SN phase. Among the cases displayed in Fig. 6 ($c_s=1\text{ km.s}^{-1}$, $\tilde{\sigma}_1(t_{em}) = 0.01\sigma_0(t_{em})$, $v(t_{em}) = 0.01V_s(t_{em})$), we see that the shell transverse collapse is achieved if, for instance, $P_h = 10^{-10}\text{ dyne.cm}^{-2}$, $N=100$ and $\eta=16$ (top panel) or if $P_h = 5 \times 10^{-10}\text{ dyne.cm}^{-2}$, $N=100$ and $\eta=10$ (middle panel). It is interesting to note that these values of η reasonably match those given by Eq. 33, for the above mentioned cases, i.e., $\langle \eta_{fg} \rangle = 12$ and $\langle \eta_{fg} \rangle = 9$, respectively. As Eq. 33 has been derived under the assumption of an exponential growth rate, this agreement a posteriori justifies its validity as a convenient estimate of the number of forming clumps in collapsing shells.

2.3.6 The shell sound speed: c_s

The development of a gravitational instability within a supershell also depends on the sound speed c_s of the shell material. Indeed, c_s is directly related to the thermal pressure P_s of the shell gas through

$$P_s = \frac{\rho_s k T_s}{\mu_s m_H} = \rho_s c_s^2. \quad (34)$$

In this equation, k and m_H are the Boltzmann constant and the hydrogen mass, respectively, while ρ_s , T_s and μ_s are the mass density, the temperature and the mean molecular weight of the shell, respectively. The larger the velocity dispersion, the more the layer resists gravitational collapse. In an H I layer ($T \simeq 100\text{ K}$, $\mu \simeq 1.3m_H$), the sound speed is $\simeq 0.8\text{ km.s}^{-1}$, while it can be as low as $\simeq 0.3\text{ km.s}^{-1}$ in an H₂ layer ($T \simeq 20\text{ K}$, $\mu \simeq 2.1m_H$) (McCray & Kafatos 1987). However, the turbulence and magnetic fields of the shell will increase these values. To some extent, they can be represented by an additional pressure term in the expression of c_s , i.e.

$$c_s = \left(\frac{kT_s}{\mu_s m_H} + \frac{B_s^2}{4\pi\rho_s} + \mathcal{T}_s \right)^{1/2} \quad (35)$$

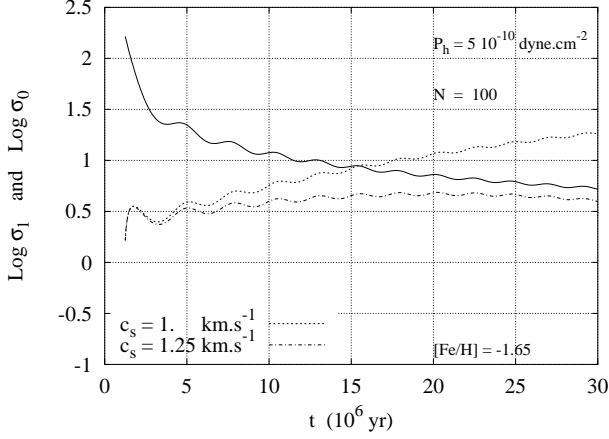


Figure 7. Temporal evolution of σ_0 (plain curve) and $\tilde{\sigma}_1$ (dashed curves), expressed in units of $1 M_{\odot} \cdot \text{pc}^{-2}$, considering the sound speeds (see the key), external pressures and SNII numbers indicated. Other parameters are $\eta=10$, $\tilde{\sigma}_1(t_{em}) = 0.01\sigma_0(t_{em})$, $v(t_{em}) = 0.01 V_s(t_{em})$

where B_s is the magnetic field in the shell and \mathcal{T}_s is the contribution of turbulence.

Figure 7 shows how highly sensible to c_s the fragmentation process is. Considering 100 SNeII and a hot background pressure of $5 \times 10^{-10} \text{ dyne.cm}^{-2}$, the fragmentation takes place even with a low initial transverse velocity, i.e. $v(t_{em}) = 0.01 V_s(t_{em})$, if $c_s = 1 \text{ km.s}^{-1}$. Increasing the latter by 25%, the transverse collapse is very weakened and the fragmentation is prevented. During the last ten million years, the evolutions with time of σ_0 and $\tilde{\sigma}_1$ are similar, that is, the evolution of $\tilde{\sigma}_1(t)$ is mostly driven by the dilution of $\sigma_0(t)$ due to the shell expansion.

Equation 35 illustrates the difficulty of estimating the sound speed of a gas. It implies the computations of its cooling history, its magnetic fields and turbulence. Moreover, the high sensibility of the fragmentation issue to c_s (see Fig. 7) shows that its value must be estimated with some accuracy. Such a task is well beyond the scope of the present work and, in what follows, we adopt $c_s = 1 \text{ km.s}^{-1}$, in agreement with many studies of supershell fragmentation (e.g. Comeron & Torra 1994, Ehlerova & Palous 2002).

3 DISCUSSION

3.1 Stars with halo GC metallicities

The previous section has shown that the shell/swept PGCC may become gravitationally unstable and finally break into fragments providing that some conditions are fulfilled, e.g. $v(t_{em})/V_s(t_{em}) \simeq 0.03$, $c_s \simeq 1 \text{ km.s}^{-1}$, $\eta \simeq \langle \eta_{fg} \rangle$. This is *not* to claim that all supershells will encounter such favourable circumstances, but one may expect that at least *some* of them will do.

Figure 8 presents the results of shell fragmentation simulations for varying values of N , P_h , η and $v(t_{em})/V_s(t_{em})$,

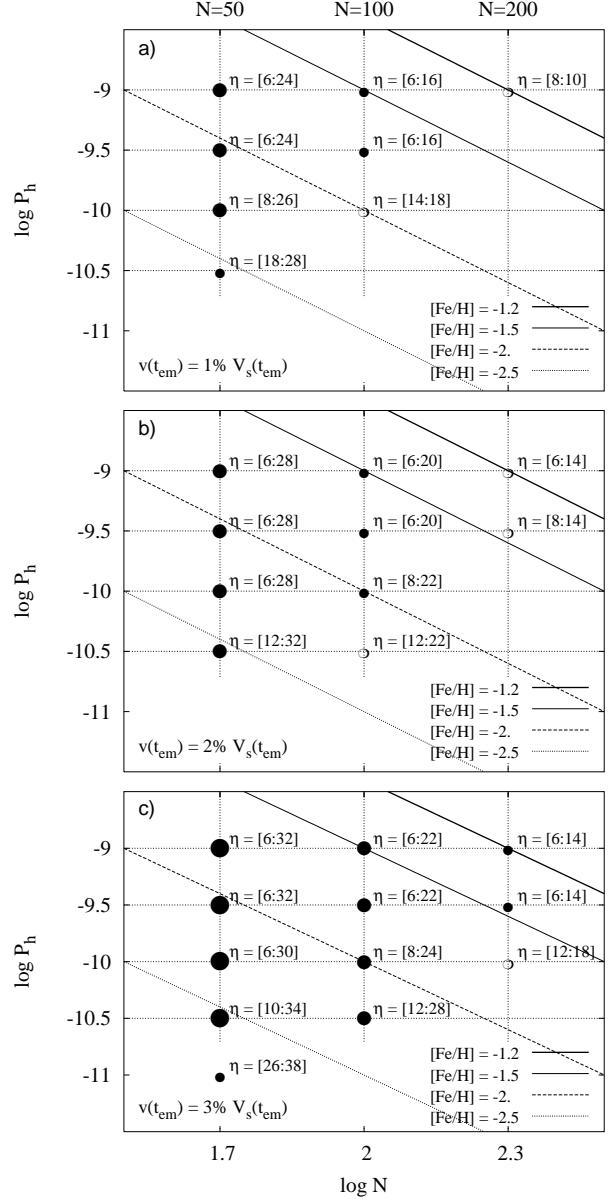


Figure 8. Summary of the $(N, P_h, v(t_{em})/V_s(t_{em}), \eta)$ values which may (open or filled circles), or may not (no symbol), lead to a swept PGCC fragmentation providing that the transverse flows converge towards the clumps embedded within the shell, i.e. $\Delta\phi = -\pi/2$. The sound speed and the initial perturbed surface density are $c_s = 1 \text{ km.s}^{-1}$ and $\sigma_1(t_{em}) = 0.01 \sigma_0(t_{em})$, respectively. The top, intermediate and bottom panels correspond to initial transverse velocity of 1, 2 and 3 per cent of the shell velocity when it emerges out of the cloud, respectively. The isometallicity curves corresponding to $[\text{Fe}/\text{H}] = -1.2, -1.5, -2, -2.5$ are also plotted, giving thus the metallicity achieved through self-enrichment for each parameter combination. For each (N, P_h) pair, 54 couples of initial perturbed velocities ($v(t_{em})/V_s(t_{em}) = 0.01, 0.02, 0.03$) and clump numbers (η ranging from 6 to 40 by step of 2) are tested. In each panel (i.e., for each value of the initial perturbed velocity), a couple (N, P_h) leading to a successful transverse collapse is marked by an open/filled circle as well as by the range of η values leading to fragmentation. The larger the range of η values, the bigger the symbol (see text for details)

assuming that $c_s=1 \text{ km.s}^{-1}$ and $\sigma_1(t_{em})=0.01 \sigma_0(t_{em})$. Five hot protogalactic background pressures ($P_h = 10^{-11}, 3.2 \times 10^{-11}, 10^{-10}, 3.2 \times 10^{-10}, 10^{-9} \text{ dyne.cm}^{-2}$) and 3 SN numbers ($N=50, 100, 200$) are tested. The upper limit for N is the maximum number of supernovae that the GC gaseous progenitor can sustain, namely $N=200$ (i.e., if $N > 200$, the absolute value of the cloud binding energy is lower than the shell kinetic energy: disruption criterion, Paper I). The lower limit is imposed by c^{PGCC} , the sound speed of the PGCC material. Indeed, the shell is “built” while sweeping the PGCC and such a mass accumulation into a shell requires the velocity of the shell to be larger than the sound speed of the ambient medium. Therefore, the lower limit to the shell velocity in the PGCC obeys:

$$V_s^{PGCC} = c^{PGCC} = \sqrt{\frac{kT}{\mu m_H}} = 8.3 \text{ km.s}^{-1} \quad (36)$$

where T and μ are the temperature ($\simeq 10^4 \text{ K}$) and the mean molecular weight ($\simeq 1.2$) of the PGCC, respectively (Fall & Rees 1985). The number of SNeII corresponding to this lower limit of the shell velocity is $N \simeq 50$ (Eq. 13, Paper I). Regarding the upper value of P_h , we refer to Murray & Lin (1992) who showed that the hot protogalactic background pressure depends on the galactocentric distance D as

$$P_h = 1.25 \times 10^{-9} D_{kpc}^{-2} \text{ dyne cm}^{-2}. \quad (37)$$

Thus, P_h is of order $10^{-9} \text{ dyne.cm}^{-2}$ in the very inner Galactic regions (i.e., $D \simeq 1 \text{ kpc}$).

In order to see what is the metallicity achieved in the shells which succeed in forming new stars, iso-metallicity curves corresponding to $[\text{Fe}/\text{H}]=-1.2, -1.5, -2$ and -2.5 (i.e., metallicities typical of the Galactic halo GCs) are displayed in each panel of Fig. 8.

For each couple (N, P_h) , 54 combinations of $v(t_{em})/V_s(t_{em})$ and η (i.e. 3 initial perturbed velocities \times 18 numbers of clumps) have been run. The initial transverse velocities correspond to 1, 2 and 3 per cent of the velocity of the shell when it enters the hot background and the number of clumps ranges from 6 to 40 by step of two. It appears that the shell is unable to fragment if $\eta \geq 40$. When a set of conditions leads to a successful fragmentation, the corresponding point in the (N, P_h) diagram is marked by a circle as well as by the range of η values leading to successful transverse collapses. Depending on whether the shell fragmentation takes place for 0 to 25 per cent, 25 to 50 per cent, 50 to 75 per cent, or 75 to 100 per cent of the number of η values tested, the corresponding triplet $(N, P_h, v(t_{em})/V_s(t_{em}))$ is marked by an open circle, a small, a median-size or a large filled circle, respectively. Figure 8 confirms that the probability of successful transverse collapse fades away with decreasing external pressure and increasing number of SNeII. As mentioned in Sect. 2.3.2, a low external pressure and a high number of SNeII leads to a larger radius for the shell, decreasing thereby its surface density (Eq. 19) and its ability to collapse.

At high pressure, i.e. $P_h \simeq 10^{-9} \text{ dyne.cm}^{-2}$, the ability of the shell to get fragmented is limited by too large a number of SNeII. Figure 8 shows however that a SN number as large as 200 does not prevent the fragmentation. Accordingly, the largest metallicity which can be achieved through

self-enrichment is $[\text{Fe}/\text{H}] \simeq -1.2$. On the other hand, at low pressure, the transverse collapse is supported by a low number of SNeII. Combining a low background pressure with the lower limit on N , Fig. 8 shows that the lowest metallicity which can be achieved is $[\text{Fe}/\text{H}] \simeq -2.8$ providing that the relative initial transverse velocity is 3 per cent. While this lower limit in metallicity is a bit uncertain, as it is achieved in the case of the highest initial transverse velocity only, the examination of the three panels in Fig. 8 clearly shows that a metallicity of $\simeq -2.5$ is actually achievable. These extreme values ($[\text{Fe}/\text{H}] \simeq -1.2$ and -2.5) match nicely the metallicities exhibited by the most metal-rich and the most metal-poor Galactic halo GCs, respectively.

At this stage, it is worth keeping in mind that the question addressed here above concerns the ability of the shell to form stars and not yet the ability of these stars to evolve into a stellar cluster. We will address the ability of the newly formed stars to form a bound cluster in a forthcoming paper and we emphasize here that, among the cases of successful fragmentation displayed by Fig. 8, some of the newly formed stars may not be able to form a bound cluster. In other words, the collapsed shells may be a source for both halo GCs and halo field stars.

Section 2.3.2 has discussed how the self-enrichment model for GC formation can shed light on the metallicity distribution of the Galactic halo. Because the parameters which determine the metallicity, i.e. N and P_h , also control the shell surface density, there is a direct link between the metallicity and the probability of star formation³. Furthermore, the initial radius and velocity of the second generation stars being the radius and the velocity of the shell at the time of their formation, their binding depends on the shell expansion law and, therefore, again, on N and P_h . As a consequence, the probability of getting a bound cluster from a shell of newly formed stars is also related to their metallicity. If we assume that a significant fraction of the field content comes from “failed GCs” (i.e. shells of stars which did not succeed in forming GCs), then these relations between the metallicity on the one hand and the probabilities of forming a second stellar generation and a bound cluster on the other hand *open the way to the computation of the metallicity distributions of both halo field stars and halo GCs*.

Since the formation of a GC requires one more condition than the shell transverse collapse (i.e. the binding of the second stellar generation), only a subset of the (N, P_h) combinations giving rise to shell fragmentation may lead to the formation of a bound cluster. Such a conclusion does not contradict, and even fits, the fact that the metallicity spectrum of halo field stars is larger than the one of GCs (e.g. Laird et al. 1988).

³ This is *not* to say that the probability of star formation is determined by the metallicity, as it can be assumed in pre-enrichment models in which the metallicity may control the star formation through line cooling processes. It rather means that the metallicity and the probability of star formation derive from the same parameters, namely the number of SNeII and the pressure of the hot protogalactic background

3.2 The very metal-poor stars ($[\text{Fe}/\text{H}] \lesssim -2.5$)

The most striking difference between the halo GC and halo field metallicity distributions resides in the much more extended metal-poor tail of the field compared to the GC system. In fact, while the most metal-poor GCs show $[\text{Fe}/\text{H}] \simeq -2.5$, the Galactic halo hosts field stars whose metallicity is much lower (e.g., CS22876-032, $[\text{Fe}/\text{H}] \simeq -3.7$, Norris, Beers & Ryan 2000). The recent discovery of HE0107-5240, the most metal-deficient star ever discovered ($[\text{Fe}/\text{H}] \simeq -5.3$, Christlieb et al. 2002) has decreased even more the lower limit of the observed metallicity distribution of halo field stars. Our model does not seem to be able to explain these very metal-poor stars (see Fig. 8) and we must therefore investigate alternative scenarios for the formation of these stars more metal-deficient than the most metal-poor GCs.

3.2.1 Isolated Type II Supernovae

The existence of very metal-poor stars has often been attributed to star formation episodes triggered by *individual* SNeII exploding in primordial gas clouds (e.g., Shigeyama & Tsujimoto 1998, Argast et al. 2000, Karlsson & Gustafsson 2001), that is, a formation scenario similar to the self-enrichment scenario for GCs except regarding the considered number of massive stars. The metallicity of such stars is determined by the ratio of the mass of metals ejected by the SNeII to the mass of hydrogen gathered by the shock wave. The SNeII yields computed by Woosley & Weaver (1995) for zero metallicity stars show that a SNeII with progenitor mass m ejects a mass of metals m_z such that $m_z \simeq 0.3m - 3.5$ (in unit of one solar mass). On the other hand, the mass M_{sw} of interstellar gas collected by the shock wave is related to the explosion energy E_0 through

$$M_{sw} = 5.1 \times 10^4 M_\odot \left(\frac{E_0}{10^{51} \text{ ergs}} \right)^{0.97}, \quad (38)$$

assuming a sound speed of 10 km.s^{-1} (or $T \sim 10^4 \text{ K}$) for the interstellar gas (Shigeyama & Tsujimoto 1998). Using these relations and assuming $E_0 = 10^{51} \text{ ergs}$ for a canonical SNeII, the metallicity achieved in shells of gas driven by isolated SNeII is straightforwardly derived (see the second column of Table 1). The explosion energy being the same whatever the SNeII progenitor mass, every SNeII sweeps the same amount of primordial circumstellar gas, irrespective of the SNeII mass (Eq. 38). Therefore, the final metallicity is determined solely by the mass of heavy elements released in the interstellar medium by the exploding star and, thus, by the SNeII progenitor mass. As a consequence, the more massive the SNeII, the larger the final metallicity. As already noticed by Shigeyama & Tsujimoto (1998), the formation of very metal-poor stars with $[\text{Fe}/\text{H}] \simeq -4$ and $[\text{Fe}/\text{H}] \simeq -2$ may therefore be ascribed to “low”-mass (i.e., $M \simeq 12 M_\odot$) and high-mass (i.e., $M \simeq 40 M_\odot$) SNeII, respectively. In order to dig out the potential link between very metal-poor stars and isolated SNeII, Shigeyama & Tsujimoto (1998) also exploited the yields of core-collapse SN predicted by nucleosynthesis calculations (e.g., Woosley & Weaver 1995, Tsujimoto et al. 1995). They focused on the abundance patterns of C, Mg, Si and Ca. The yields of these elements being not (or at least less) affected by the mass-cut issue, they should therefore be known with a better accuracy than

the yields of heavier elements such as the iron peak ones. They noticed the good agreement between the abundance patterns arising in the remnants of first generation SNeII, as predicted by nucleosynthesis calculations, and those inferred from the spectra of halo stars with $[\text{Fe}/\text{H}] \lesssim -2.5$. As a result, Shigeyama & Tsujimoto (1998) suggested that very metal-poor stars actually formed out of interstellar gas which had been swept by isolated SNeII. They also note that the large observational scatter in the abundance ratios among these stars can be explained by the differences in SNeII yields with the mass of the progenitor.

It is worthy of a mention that such isolated SNeII are certainly not able to trigger the formation of GCs owing to the small amount of interstellar gas swept by the blast wave (Eq. 38; also, not all the gas will be converted into stars). Should such low-mass halo clusters have managed to form however, they will have been quickly destroyed by the Galactic tidal fields, low-mass clusters being among the most vulnerable in this respect (e.g., Gnedin & Ostriker 1997). Therefore, this extension of the self-enrichment scenario to single SNeII explosions does not contradict the absence of Galactic halo GCs with $[\text{Fe}/\text{H}] \lesssim -2.5$.

3.2.2 Hypernovae

In fact, even stars as massive as $40 M_\odot$ may trigger the formation of stars with a metallicity as low as -4 , providing that they explode as *hypernovae*, i.e., supernovae characterized by explosion energies of order $E_0 \sim 10^{52} - 10^{53} \text{ ergs}$. This class of objects includes two categories depending on the progenitor mass, namely core-collapse hypernovae and pair-instability hypernovae. They both have been invoked as possible explanations to peculiar abundance patterns observed in some very metal-poor field stars.

Core-collapse hypernovae. Recent observations suggest that at least some core-collapse supernovae explode with explosion energies ten to one hundred times higher than the energy released by a canonical SNeII (e.g., Galama et al. 1998). They likely originate from relatively massive star ($M \gtrsim 25 M_\odot$). In contrast to pair-instability hypernovae (see below), the mass range of their progenitor is thus similar to the one of canonical SNeII.

If hypernovae occurred in the early stage of the Galactic evolution and induced star formation, their abundance pattern may still be observable in the atmospheres of some low-mass halo stars. As for the case of star formation triggered by single SNeII, we can derive an estimate of the metallicity of these halo stars using Eq. 38 and hypernova yields. Nakamura et al. (2001) have investigated in detail the nucleosynthesis of core-collapse hypernovae and compared it with the yields of canonical (i.e., $E_0 \sim 10^{51} \text{ ergs}$) core-collapse SNeII with similar progenitor mass. Their Tables 2-5 show that SNeII and hypernovae with similar progenitor mass release much the same amount of metals. The resulting metallicity of stars formed in hypernova remnants are given in Table 1, following the same of line of reasoning as in the previous section. Hypernovae being much more energetic than SNeII, and the mass of interstellar gas swept by the blast wave being roughly proportional to the explosion energy (Eq. 38), they will collect a larger amount of interstellar gas. Therefore, should core-collapse hypernovae be able to trigger the

Table 1. Dependence of the metallicity [Fe/H] on the progenitor mass m and explosion energy E_0 of supernovae (SN; $E_0 = 10^{51}$ ergs) and hypernovae (HN; $E_0 = 10$ or 100×10^{51} ergs). Every mass is expressed in units of one solar mass. (1) A $12 M_\odot$ star explodes as a canonical SNII. According to Nakamura et al. (2001), stars less massive than $25 M_\odot$ do not explode as core-collapse hypernovae and such cases are thus not considered in this Table. (2-3) More massive stars explode either as core-collapse supernovae or core-collapse hypernovae. (4) Very massive objects (i.e., $M > 100 M_\odot$) explode as pair-instability hypernovae. M_{sw} , the mass of interstellar gas collected by the explosion blast wave, depends on the explosion energy through Eq. 38. m_z is the mass of metals released by an exploding massive star with progenitor mass m . The metallicity [Fe/H] is derived assuming that the mass m_z of metals is mixed with the mass M_{sw} of collected interstellar gas

$E_0/10^{51}$ ergs	1 (SN)	10 (HN)	100 (HN)
M_{sw}	5.1×10^4	5.1×10^5	5.1×10^6
(1) $(m, m_z)=(12, 0.1)$ [Fe/H] \simeq	-4	-	-
(2) $(m, m_z)=(25, 4)$ [Fe/H] \simeq	-2.4	-3.4	-4.4
(3) $(m, m_z)=(40, 10)$ [Fe/H] \simeq	-2.1	-3.1	-4.1
(4) $(m, m_z)=(200, 100)$ [Fe/H] \simeq	-	-2.0	-3.0

formation of new stars, these stars will be more metal-poor than the ones formed in the remnants of canonical SNeII. Thus, they may be well-suited to explain the formation of stars with a metallicity as low as [Fe/H] $\simeq -4$ (see Table 1).

The most significant feature of hypernova nucleosynthesis is their iron production, this one being larger than in SNeII by a factor 2 to 10 (Nakamura et al. 2001). This leads to small abundance ratios of α elements over iron. Nakamura et al. (2001) thus suggested that the gas out of which the very metal-poor binary CS 22873-139 ([Fe/H] = -3.4) formed had been contaminated by the ejecta of an hypernova as this halo star shows almost solar [Mg/Fe] and [Ca/Fe] ratios. On the other hand, while stars with $-2.5 \lesssim [\text{Fe}/\text{H}] \lesssim 0$ show [Zn/Fe] $\simeq 0$ (e.g., Primas et al. 2000), this abundance ratio is steadily increasing towards [Zn/Fe] ~ 0.5 as the metallicity decreases, for stars more metal-poor than [Fe/H] ~ -2.5 (e.g., Cayrel et al. 2003). Umeda & Nomoto (2002) notice that such a large [Zn/Fe] ratio arises naturally in their own hypernova model and thus conclude that core-collapse hypernovae are likely to have contributed to the early Galactic chemical evolution.

Pair instability hypernovae. These very massive ($\simeq 140$ - $260 M_\odot$) objects exploding with $E \gtrsim 10^{52}$ ergs, they are also called hypernovae. Their name (i.e., “pair instability”) refers to the electron-positron pair instability process encountered during the central oxygen-burning stages (see Umeda & Nomoto 2002, their appendix for a detailed description).

The main feature of these very massive stars is their ability to “pass carbon and oxygen from the helium-burning

core through the hydrogen-burning shell, in such a way that it is CNO processed to nitrogen before entering the hydrogen envelope” (Carr, Bond & Arnett 1984). These stars thus produce large supersolar values of N/Fe, an effect not predicted by models of Galactic chemical enrichment based on stars less massive than $100 M_\odot$. Following their discovery of CS 22949-037, a very metal-poor star ([Fe/H] = -3.8) showing extreme nitrogen enhancement ([N/Fe] = 2.3), Norris et al. (2002) suggested that this star may have been formed out of gas polluted and compressed by such a very massive hypernova.

On the other hand, in marked contrast with core-collapse hypernova yields, Umeda & Nomoto (2002) quote that pair-instability hypernovae are unlikely to produce [Zn/Fe] ratios as large as in very metal-poor stars where [Zn/Fe] ranges from solar up to $\simeq 0.5$ (Cayrel et al. 2003). Actually, the abundance ratio derived from their hypernova yields is of order [Zn/Fe] = -1.5, that is, 1 to 2 dex smaller than in very metal-poor stars. Additionally, Heger & Woosley (2002) note the absence of the r-process in these massive objects, which conflicts with observations showing appreciable amounts of r-process elements in very metal-poor stars (e.g., Burris et al. 2000). Based on these two arguments, i.e., the low abundance ratio [Zn/Fe] as well as the absence of r-process elements in pair instability hypernova ejecta, Umeda & Nomoto (2002) and Heger & Woosley (2002) conclude that the abundances of very metal-poor stars cannot be ascribed to pair instability hypernovae only and must include the contribution of an additional nucleosynthetic component, namely those lower mass stars that make “regular” supernovae. We also note that pair-instability hypernovae release fairly large amounts of metals in the interstellar medium, of order $100 M_\odot$ (Umeda & Nomoto 2002, their Tables 15-18). In fact, these stars disrupt completely when exploding, leaving no compact remnant after the explosion (i.e., no issue of “mass-cut” or “fall-back”, see Heger & Woosley 2002). The mixing of so large an amount of metals with a mass of primordial gas of $\simeq 5 \times 10^5 M_\odot$ ($E_0 = 10 \times 10^{51}$ ergs) or $\simeq 5 \times 10^6 M_\odot$ ($E_0 = 100 \times 10^{51}$ ergs) will lead to metallicities of order [Fe/H] $\simeq -2$ or [Fe/H] $\simeq -3$, respectively. Therefore, the metallicity of the most metal-poor stars in the Galactic halo cannot be explained by pair-instability hypernovae.

3.2.3 Single short-acting source of energy and triggered star formation

The issue of whether isolated exploding massive or very massive stars can stimulate the formation of new stars in the layers of interstellar gas they have swept is not explicitly addressed in the papers mentioned in Sect. 3.2.1 and 3.2.2 (e.g., Shigeyama & Tsujimoto 1998, Argast et al. 2000, Norris et al. 2002). It is merely assumed that such stimulated star formation actually took place during the early Galactic stages.

The model presented in this paper (see sect. 2) is not the most appropriate to address this issue quantitatively as it deals with a continuous input energy and not with a single short-acting source of energy. Actually, supershells created in connection to single explosion and those created around a cluster of massive stars do not show the same expansion rate

with time (see below). We have seen in Sect. 2 how the radius and the velocity of the shell affect its ability to collapse through the shell surface density and the stretching of the forming perturbation, respectively. Hence, to solve the issue of whether a single supernova/hypernova triggers the formation of new stars requires to derive a new temporal evolution of the shell radius, in the PGCC and in the protogalactic background, adequate to single explosion. This is beyond the scope of the present paper whose main goal is to address the formation of stars with $-2.5 \lesssim [\text{Fe}/\text{H}] \lesssim -1$ (i.e., the metallicity range of halo GCs). Some qualitative inferences can however be made. Efremov, Ehlerova & Palous (1999) compared the propagation in an homogeneous medium of both kinds of supershells. In case of an abrupt energy input, the early expansion of the supershell proceeds at a higher velocity than in the case of a continuous input of the same energy amount. Accordingly, in the former case, the shell of swept gas is more strongly stretched and this hampers the formation of an initial perturbation. After a few millions years however, the shell created in connection to an abrupt energy input slows down and shows both a radius and a velocity lower than in case of a continuous energy input. In contrast to the initial shell expansion, this second stage favours the transverse collapse through a larger shell surface density and a weaker stretching of the shell perturbed regions. Whether the collapse will occur is actually not certain. The source of the energy input being point-like (i.e., its size is much smaller than the one of a cluster of massive stars), the initial amplitude of the transverse motions within the shell will be lowered accordingly, thus reducing the collapse.

Comparing SNeII and hypernovae, hypernovae sweep a larger amount of gas thanks to their larger energy input (Eq. 38). However, this also leads to a larger shell radius. Both effects acting on the shell surface density in opposite ways, only detail computations will tell us which class of objects is the most efficient in forming new stars. A $E_0 \sim 2 \times 10^{52}$ ergs hypernova being able to collect amount of gas as large as $10^6 M_\odot$ (Eq. 38), one might think that pair-instability hypernovae could be related to the formation of GCs, at least the most metal-poor ones as such hypernovae can chemically enrich the initially pristine gas up to $[\text{Fe}/\text{H}] \simeq -2$ (see Table 1). However, the $[\text{Zn}/\text{Fe}]$ abundance ratio predicted for hypernova ejecta (i.e., $[\text{Zn}/\text{Fe}] < -1.5$, Umeda & Nomoto 2002) shows a sharp discrepancy with the roughly solar value observed in halo field stars with $[\text{Fe}/\text{H}] \simeq -2$ (Primas et al. 2000) as well as in NGC6397, a halo GC with the same metallicity (Thevenin et al. 2001). Therefore, the abundance patterns of stars in this metallicity range cannot be ascribed to pair-instability hypernovae.

Obviously, it is not straightforward to conclude whether single massive star explosions are able to trigger the formation of new stars. More computations are required to answer a question which is certainly worthy of further investigation owing to its potential link with very metal-poor stars.

3.2.4 External pollution onto PopIII stars

Shigeyama, Tsujimoto & Yoshii (2003) have recently suggested that some very metal-deficient stars may have been born as metal-free (PopIII) stars whose external layers were afterwards polluted by the accretion of chemically enriched

interstellar gas. The metallicity achieved by the external layers will depend on the metallicity and mass of the accreted gas, as well as on the stellar mass fraction with which the accreted gas has been mixed. As a consequence, the chemical enrichment of stellar superficial layers will show up more markedly in main sequence stars than in red giants, the convective envelope (i.e. the mixing zone) being almost two orders of magnitude larger in halo giants (about half the star mass) than in non-evolved metal-poor stars (about one per cent of the star mass). Shigeyama et al. (2003) have shown that the extremely low metallicity ($[\text{Fe}/\text{H}] \simeq -5.3$) of the giant HE0107-5240 (Christlieb et al. 2002) may originate from such a mechanism, that is, an external pollution while the star was on the main sequence followed by the dilution of the accreted material as the star started ascending the red giant branch. Owing to their thin convective envelopes, polluted Pop III stars still on the main sequence would exhibit larger metallicities, i.e. of order $[\text{Fe}/\text{H}] \simeq -3$, although still lower than the most metal-poor GCs.

3.2.5 Star formation in dwarf galaxies

Within the frame of a hierarchical model for halo formation, Cote et al. (1999) proposed that the excess of very metal-poor field stars with respect to GCs was formed in the most metal-deficient dwarf galaxies trapped within the Galactic potential well. These galaxies are not expected to contribute to the GC population. Indeed, due to the luminosity-metallicity correlation observed among dwarf galaxies (Gilmore 2000, Mateo 2000), the most metal-poor dwarfs are also expected to be the least luminous. Dwarf galaxies exhibit a luminosity threshold for hosting a GC system. For instance, the Fornax dwarf spheroidal galaxy is the faintest ($M_v \simeq -12.3$, Harris 1991) galaxy known to harbour its own GC system. Therefore, the dimmest dwarf galaxies, which are also the most metal-poor, may have contributed to the halo field and not to the halo GC system.

4 CAVEATS AND FUTURE WORK

It is worthy of a mention that the model results presented above constitute a first and preliminary step in our computations of globular cluster star formation. In fact, several aspects are still to be worked out. We now give some examples of these, which our future developments will have to encompass.

- As the shell collapse is followed until the perturbed and unperturbed surface densities reach similar values, a non-linear model would better describe the growth with time of the shell fragments. In this respect, we note that Wunsch & Palous (2001) studied the transverse collapse of supershells propagating in the Galactic disc using both linear and non-linear models. The comparison of the results obtained in both cases, and for instance the time at which the shell gets fragmented, does not show significantly different results.

- At some moments of its propagation through the hot protogalactic background, the shell undergoes transient accelerations (see Figs. 1 and 2) which may lead to Rayleigh-Taylor instabilities. Rayleigh-Taylor instabilities take place

when a cold, dense gas (i.e. the supershell) is accelerated by pressure from a hot more rarefied gas (i.e. the bubble). Spikes and globules of the colder fluid will tend to penetrate the warmer fluid (Spitzer 1978). While this effect may disrupt the shell and, thus, prevent the process of triggered star formation, it can also lead to local overdensities in the shell material, accelerating thereby star formation. It will therefore be of interest to estimate whether the shell transient accelerations may trigger Rayleigh-Taylor instabilities, how far these ones develop and how the process of stimulated star formation within the shell is affected.

- The computation of the shell expansion law can still be improved as it does not yet include energy losses, such as those induced by viscous processes. For given number of SNeII and external pressure, these effects may lower the radius of the shell with respect to what has been computed in Sect. 2.2 and, thus, increase the shell surface density and the probability of star formation. If the formation of stars may be triggered even at pressures lower than $P_h = 10^{-11}$ dyne.cm⁻², metallicities lower than $[\text{Fe}/\text{H}] \simeq -2.8$ may be achieved.

5 SUMMARY

This paper has presented the results of simulations dedicated to the transverse collapse of shells of gas resulting from the sweeping of gaseous GC progenitors by SNeII. In these simulations, the growth of an initial perturbation in the shell surface density is followed by solving the linear perturbed equations of continuity and motion for transverse flows in a spherical shell of gas. Such a collapse depends on several parameters, namely the number of SNeII, the background pressure, the sound speed of the shell gas and the initial conditions of the perturbation (i.e. the number of clumps, the initial perturbed surface density and velocity and the corresponding phase difference). All these parameters have been discussed in turn. The results show that the pressure P_h of the hot protogalactic background ($P_h \sim 10^{-10}$ dyne.cm⁻², Fall & Rees 1985, Murray & Lin 1992) and the numbers N of SNeII allowed by the disruption criterion (i.e. smaller than 200, Paper I) can indeed lead to a successful shell transverse collapse, and thereby to the formation of new stars, assuming some reasonable initial conditions for the perturbation (see Fig. 8). The metallicities achieved in the shells able to collapse agrees with the metallicity range of Galactic halo GCs, namely, $-2.5 \lesssim [\text{Fe}/\text{H}] \lesssim -1$. Furthermore, while N and P_h determine the metallicity achieved through self-enrichment, they also control the probability of triggered star formation and the ability of these second generation stars to form a bound GC. Such a property is the most interesting since it opens the way to the understanding of the halo metallicity distribution functions, for both stars and clusters.

This paper has been typeset from a \TeX / \LaTeX file prepared by the author.

ACKNOWLEDGMENTS

I am grateful to Richard Scuflaire for fruitful advices and discussions. Supports from Pôle d'Attraction Interuniversitaire through grant P5/36 (SSTC, Belgium) and from the European Commission through grant HPMT-CT-2000-00132 are gratefully acknowledged.

REFERENCES

- Abel T., Bryan G.L., Norman M.L., 2002, *Science*, 295, 93
 Argast D., Samland M., Gerhard O.E., Thielemann F.-K., 2000, *A&A*, 356, 873
 Bromm V., Coppi P.S., Larson R.B., 1999, *ApJL*, 527, 5
 Brown J.H., Burkert A., Truran J.W. 1991, *ApJ* 376, 115
 Brown J.H., Burkert A., Truran J.W. 1995, *ApJ* 440, 666
 Burris D.L., Pilachowski C.A., Armandroff T.E., Sneden C., Cowan J.J., Roe H., 2000, *ApJ*, 544, 302
 Campbell B., Hunter D.A., Holtzman J.A., Lauer T.R., Shayer E.J., Code A., Faber S.M., Groth E.J., Light R.M., Lynds R., O'Neil E. Jr., Westphal J.A. 1992, *AJ* 104, 1721
 Carr B.J., Bond J.R. & Arnett W.D. 1984, *ApJ* 277, 445
 Castor J., McCray R., Weaver R., 1975, *ApJ* 200, L107
 Cayrel R. 1986, *A&A* 168, 81
 Cayrel R., Depagne E., Spite M., Hill V., Spite F., Francois P., Plez B., Beers T., Primas F., Andersen J., Barbuy B., Bonifacio P., Molaro P., Nordstrom B., 2003, *A&A*, accepted for publication
 Christlieb N., Bessell M.S., Beers T.C., Gustafsson B., Korn A., Barklem P.S., Karlsson T., Mizuno-Wiedner M., Rossi S. 2002, *Nature* 419, 904
 Christlieb N., Gustafsson B., Korn A., Barklem P.S., Beers T.C., Bessell M.S., Karlsson T., Mizuno-Wiedner M., 2003, *ApJ*, accepted for publication
 Comeron F., Torra J. 1994, *ApJ* 423, 652
 Cote P. 1999, *AJ* 118, 406
 Dinge D., 1997, *ApJ*, 479, 792
 Efremov Y.N., Elmegreen B.G. 1998, *MNRAS* 299, 643
 Efremov Yu.N., Ehlerova S., Palous J. 1999, *A&A* 350, 475
 Ehlerova S. & Palous J. 2002, *MNRAS* 330, 1022
 Elmegreen B.G. 1994, *ApJ* 427, 384
 Fall S.M., Rees M.J. 1985, *ApJ* 298, 18
 Galama T., et al. 1998, *Nature* 395, 670
 Gilmore, G. 2000, in ASP Conf. Ser. 230, *Galaxy Disks and Disk Galaxies*, eds. J.G. Funes & E.M. Corsini, 3
 Gnedin O.Y., Ostriker J.P., 1997, *ApJ*, 474, 223
 Harris, W.E. 1991, *ARA&A*, 29, 543
 Harris W.E., Pudritz R.E. 1994, *ApJ* 429, 177
 Heger A. & Woosley S.E. 2002, *ApJ* 567, 532
 Karlsson T. & Gustafsson B. 2001, *A&A* 379, 461
 Kennicutt R.C. Jr. 1989, *ApJ* 344, 685
 Lada E.A., Strom K.M., Myers P.C., 1993, in: *Protostars and planets III*, p245
 Laird, J.B., Carney B.W. & Latham D.W. 1988, *ApJ* 95, 1843
 Larson R.B. 1988, in: *The Harlow-Shapley Symposium on Globular Cluster Systems in Galaxies*, eds. Grindley J.E. & Davis Philip A.G., Dordrecht, Kluwer Academic Publishers, p311
 Mateo, M. 2000, in *The First Stars (Proceedings of the MPA/ESO Workshop held at Garching, Germany, 4-6 August 1999)*, eds. A. Weiss, T.G. Abel & V. Hill, Springer, 283
 McCray R., Kafatos M. 1987, *ApJ* 317, 190
 Murray S.D., Lin D.N.C. 1992, *ApJ* 400, 265
 Nakamura F., Umemura M., 1999, *ApJ*, 515, 239
 Nakamura T., Umeda H., Iwamoto K., Nomoto K., Hashimoto M., Hix W.R., Thielemann F.-K. 2001, *ApJ* 555, 880
 Nakamura F., Umemura M., 2001, *ApJ*, 548, 19
 Norris J.E., Beers T.C. and Ryan S.G. 2000, *ApJ* 540, 456

- Norris J.E., Ryan S.G., Beers T.C., Aoki W. & Ando H. 2002, ApJL 569, 107
- Opik E.J. 1953, IrAJ 2, 2190
- Palla F., Salpeter E.E., Stahler S.W., 1983, ApJ, 271, 632
- Parmentier G., Jehin E., Magain P., Neuforge C., Noels A., Thoul A.A. 1999, A&A 352, 138 (Paper I)
- Parmentier, G., Jehin, E., Magain, P., Noels, A., & Thoul, A. 2000, A&A, 363, 526
- Parmentier G. & Gilmore G. 2001, A&A 378, 97
- Primas F., Brugamyer E., Sneden C., King J.R., Beers T.C., Boesgaard A.M. & Deliyannis C.P. 2000, in: The First Stars, eds. Weiss A., et al., Springer, p51
- Rosenberg A., Saviane I., Piotto G., Aparicio A., 1999, AJ, 118, 2306
- Rubio M., Barba R.H., Walborn N.R., Probst R.G., Garcia J., Roth M.R. 1998, AJ 116, 1708
- Shigeyama T., Tsujimoto T. & Yoshii, Y. 2003, ApJL 586, 57
- Smith G.H., 1999, ApJL, 526, 21
- Spitzer L. 1978, Physical Processes in the Interstellar Medium, Wiley-InterScience
- Thevenin F., Charbonnel C., de Freitas Pacheco J.A., Idiart T.P., Jasniewicz G., de Laverny P. and Plez B. 2001, A&A 373, 905
- Tsujimoto T., Nomoto, K., Yoshii Y., Hashimoto M., Yanagida S. and Thielemann F.-K. 1995, MNRAS 277, 945
- Shigeyama T. & Tsujimoto T. 1998, ApJL 507, 135
- Tsujimoto T, Shigeyama T., Yoshii Y. 1999, ApJL 519, 63
- Umeda H. & Nomoto K. 2002, ApJ 565, 385
- Vietri M., Pesce E., 1995, ApJ, 442, 618
- Wasserburg G.J. & Qian Y.-Z. 2000, ApJL 531, 33
- Walter F., Kerp J., Neb D., Brinks E., Klein U., 1998, ApJ, 502, L143
- Weaver R., McCray, R., Castor, J., 1977, ApJ 218, 377
- Woosley S.E. & Weaver T.A. 1995, ApJS 101, 181
- Wunsch R. & Palous J. 2001, A&A 374, 746
- Zinn R. 1985, ApJ 293, 424